Dusty Galaxies: Modeling Infrared Spectra from Heavily Obscured Objects

I give permission for public access to my Honors paper
and for any copying or digitization to be done at the discretion
of the College Archivist and/or the College Librarian.

Signed:_____

Full Name:_____Vincent Franklin Viola_____

Date: _____

Dusty Galaxies:
Modeling Infrared Spectra from Heavily Obscured Objects

Vincent Franklin Viola

Department of Physics
Rhodes College
Memphis, TN

2015

Submitted in partial fulfillment of the requirement
for the Bachelor of Science degree with Honors in Physics

This Honors paper by Vincent Franklin Viola has been

read and approved for Honors in Physics.

Dr. David Rupke

Project Advisor

_____

Dr. Benjamin Purkis

Extra-Departmental Reader

_____

Dr. Brent Hoffmeister

Department Chair

_____

Table of Contents

List of Figures……..v

Abstract……..…vii

Chapter 1: Introduction……1

Chapter 2: Spectroscopy and Source Data……...4

Chapter 3: Polycyclic Aromatic Hydrocarbons…….10

Chapter 4: Fitting the Spectra……18

Chapter 5: Results and Statistical Analysis……...25

Chapter 6: Summary and Conclusions……..38

Works Cited……..40

List of Figures

Figure Number	Figure Title	Page
2.1	Visual representation of the concept of visual extinction	6
2.2	Plot of blackbody radiation at various temperatures	8
3.1	Plot of PAH templates	13
3.2	Plot of an example Lorentzian/Drude Profile	15
3.3	Example of measuring Equivalent Width	17
4.1	Example fit of IRAS F17252+3659	21
4.2	Comparison plot of extinction curves	24
5.1	Comparison plot of a galaxy fit with both extinction curves	25
5.2	Fit of AM 1925-724 NED02	26
5.3	Fit of 2MASX J14572285+3846376	27
5.4	Fit of 2MASX J14262392+3244361	28
5.5	Fit of IRAS F14351+3553	29
5.6	Fit of SDSS J160508.46+544729.9	30

5.7	Fit of 2MASX J06210118-6417238	31
5.8	SDSS J121346.07+02481.4	32
5.9	SDSS J162625.94+221146.4	33
6.1	Histogram of Black Body Temperatures	35
6.2	Histogram of Silicate Extinction of Black Bodies	36
6.3	Histogram of Water Ice Absorption of Black Bodies	37

ABSTRACT

Dusty Galaxies: Modeling Infrared Spectra from Heavily Obscured Objects

By

Vincent Franklin Viola

We fit models to heavily obscured infrared spectra taken by the Spitzer Space Telescope and prepare them for cataloguing in the Infrared Database of Extragalactic Observables from Spitzer (IDEOS). The software we use, QUESTFIT, models the spectra using up to three extincted blackbodies (including silicate, water ice, and hydrocarbon absorption) and PAH templates. We present results from a sample of the approximately 200 heavily obscured spectra that will be present in IDEOS. We will explore some of the physical properties of the various types of dust, such as their mechanisms for emission and absorption. Based on our results, we can draw conclusions as to the nature of absorbing material surrounding the galaxies, as well as potential domination by active galactic nuclei or starbursts.

Chapter 1: Introduction

Galaxies are often obscured by a variety of dust grains, such as carbonaceous dust and silicate dust, which absorb and scatter much of the light emitted by the galaxies. Carbonaceous dust in particular absorbs most of the obscured light from the x-ray, ultraviolet, and optical spectrums and reemits it as infrared light. Since this shroud of carbonaceous dust has absorbed the majority of the galaxy's light isotropically, that is, without regard to direction or angle of incidence, we can model it as an idealized physical body, which we call a black body. The given range of wavelengths at which a black body radiates most strongly is based on its temperature. This carbonaceous dust reaches a temperature from receiving energy from the irradiance of the galaxies that it obscures that causes it to emit a spectrum most strongly in the infrared from 1 μm to 100 μm. Thus, the most efficient means of observing the galaxy is through infrared telescopes. The targets in our project were observed with the Spitzer Space Telescope, which is a space telescope that functions most effectively in the near to far infrared. The Spitzer Space Telescope provided the most efficient means for accurately observing extragalactic observables in the mid to far infrared, while circumventing the difficulties of making observations on Earth. Ground based observatories have certain inconveniences associated with them, with the most important one being that earth's atmosphere completely obscures certain infrared wavelengths. Additionally, all telescopes have the issue that they themselves act as objects that emit strongly enough in the infrared, and thus the instrument itself becomes a source of noise in the data. Thus, when Spitzer was cryogenically cooled, it bypassed these issues since it was also above the Earth's atmosphere. Therefore, it was able to make much more sensitive infrared observations than ground based telescopes.

Along with carbonaceous dust, there are many other atoms, molecules and chemical compounds that contribute to galactic spectra. Among other important emitters in the mid-IR are polycyclic-aromatic hydrocarbons (PAHs). PAHs are comprised of carbon and hydrogen, and each compound has multiple atomic rings. Instead of obscuring all light and reemitting it as a black body, PAHs become excited after they absorb either an optical photon or an ultraviolet (UV) photon (Leger & Puget 1984; Allamandola 1985, 1989). After entering an excited state, they then reemit photons of their own. Excited PAHs most frequently reemit photons at 3.3, 6.2, 7.7, 8.6, 11.2 and 12.7 μm, as well as at longer wavelengths, all of which are in the near to mid infrared range. While both optical and UV photons excite PAHs, far-UV photons most frequently interact with PAHs in the star formation region of these galaxies. Therefore, since the strength of PAH emission features is directly correlated to the amount of absorbed light from star formation, these PAH emissions can be used to draw conclusions on the amount of star formation occurring in a galaxy. (Peeters, Spoon & Tielens 2004)

Molecular ice and silicate dust grains, another type of dust made up of silicon and oxygen, absorb some infrared emissions, in contrast to the two afore mentioned types of emitting. Silicates absorb infrared emission when their Si-O bonds bend and stretch due to vibrations from being heated up over >150 K. Similarly, water ice absorbs infrared emission when its O-H bonds bend and stretch. Silicate absorption features can be found over the entire range of the spectra, but is focused at 9.8 μm. Water ice absorption is focused at 6 μm (Spoon et al. 2001, 2004, 2005). Depending on the strength of the water ice absorption feature, it can tell us whether or not there are cold molecular clouds obscuring the target.

The spectra observed via the Spitzer Space Telescope were processed and uploaded to the Cornell Atlas of Spitzer/IRS Sources, which is a spectral catalogue of over 13,000

homogenously reduced, low-resolution observations of fixed objects from the Spitzer Space telescope. We have fit 199 of these spectra in order to extract physical parameters that provide information about the emission and absorption features. Instances of these parameters include blackbody temperatures, extinction values, PAH fluxes and water ice absorptions. We hope to make various classifications regarding the nature of the galaxies based on statistical analyses of these parameters and comparison to other samples of obscured galaxies in the literature.

Some of the important classifications we seek are composition of absorbing material and classification of active galactic nuclei (AGN) by most active contributions. In determining classification of an AGN, correlation between extinction and PAH equivalent width determines the activity of the AGN in comparison to domination of starbursts within the galaxy. Targets that have large PAH equivalent widths and small extinctions are most heavily dominated by starbursts, whereas objects with smaller PAH equivalent widths and bigger extinctions have much more AGN contribution, but are still mostly dominated by starbursts. Finally, when both the PAH equivalent width and extinction are tiny, the AGN must be as powerful as or more so than the starbursts (Veilleux et al. 2009). Additionally, correlations between silicate absorptions and water ice absorption with HCN and C_2H_2 can provide insight as to the structure of absorbing material. Strong correlation between these features shows that the composition of the absorbing material is similar between targets, whereas loose correlation means there is significant diversity in the structure of absorbing material (Veilleux et al. 2009).

Chapter 2: Spectroscopy and Source Data Background

We retrieved our spectra from the Cornell Atlas of Spitzer-IRS Sources (CASSIS), which is the database containing the majority of low resolution spectra taken by the Spitzer space telescope during its mission These spectra were taken using the two low resolution infrared spectrometer (IRS) modules of Spitzer: the short-low module (SL), which operates from 5.3–14 μm, and the long-low module (LL), operating from 14–38 μm. The CASSIS database has ~12,000 low-resolution spectra of both sources that are moving, and of stationary sources. The spectra were taken using two different modes (IDEOS proposal). One of these is staring mode, which is the standard means of operating a spectrometer. A target would remain the focus of one of the IRS slits for a designated amount of time in order to observe it and record the spectra, usually varying between anywhere from a minute to six minutes (IRS Instrument handbook). In contrast, cluster mode, also known as mapping mode, allows for a user to record spectra at various points around a central target via a configured grid around surrounding the central target (IRS Instrument handbook). CASSIS contains low-resolution high quality spectra for the entirety of the staring mode spectra. However, CASSIS includes many cluster mode spectra as well.

The CASSIS spectra were extracted using an optimal extraction algorithm developed by the IRS team at Cornell, which is a noteworthy contrasting to the normal tapered column extraction or full slit extraction methods typically used. While the details are not crucial to our understanding, it is important to note that the extraction method was tailored to the fact that our extragalactic targets are sometimes very far away, and thus their signal can often be hard to distinguish from background noise signals coming from other sources that are not the target. So, in order to optimize the ratio of the target's signal to the background noise, (signal-to-noise, or

S/N), the optimal extraction algorithm was developed to weight the signal from some fainter galaxies more heavily.

We have fit 199 spectra of the 4276 extragalactic sources that are a part of CASSIS database. The spectra we fit are not only characterized by most heavily emitting between the 1-100 μm range, but also that they are the most heavily extincted of the spectra that are a part of CASSIS. What this means is that these galaxies had the more of their light either absorbed or scattered than any of the other galaxies. We describe the optical depth of "columns" of space between the observing instrument and the target. Optical depth is mathematically described by the following equation:

$$\tau = \int_0^z K dz = N\sigma \tag{2.1}$$

The first portion of this equation describes taking the density of sections along a length of the column, with K being the coefficient of extinction, and z the length of the whole column. Another way to think about K is that it is the amount of absorption and scattering per unit length, which is proportional to the number of particles present in the column. Integration is necessary since one would be adding up the amount of particles per infinitesimal strip of space for the entirety of the column. The second half of the equation assumes K is independent of Z and gives τ in terms of N, the column density (units of particles/cm^2), and σ, the cross section (units of cm^2), for absorption and scattering.

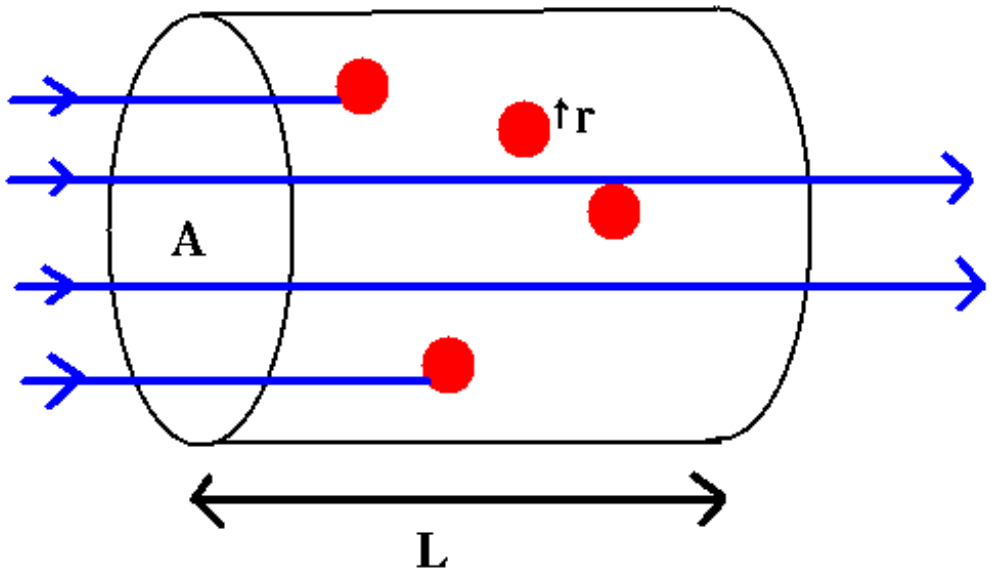

Figure (2.1): A visual representation of optical depth and the scattering of photons as they collide with dust particles. Red dots are the particles, blue lines are the photons, L is the column length and A is the "screen" of extinction. The way this schematic relates to our equations is that A would be equivalent to σ, and L would be equivalent to the full length z. While r, the size of the absorbers or scattering particles, is not directly in our equation, we can assume that K and N would be directly proportional to r, as well as number of absorbers. (http://burro.astr.cwru.edu/Academics/Astr221/StarPhys/opticaldepthprimer.html).

The way we mathematically describe how much of the intensity of the original signal is lost is through the following:

$$I_\lambda = I_{\lambda,0} e^{-\tau_\lambda} \tag{2.2}$$

I_λ is the intensity with obscuration factored in, $I_{\lambda,0}$ is the original intensity, τ_λ is the optical depth, and e is Euler's number. So, one can see that the amount of light received decreases exponentially with optical depth. This means that for the majority of our spectra, the vast majority of the electromagnetic radiation in the visual wavelengths is lost due to scattering and absorption. The optical depth for infrared emission is much lower, which is why these galaxies are best observed by the Spitzer IRS instruments. To provide a potential point of reference, the

extinction in the visual band is measured in units of A_V, and A_V~1 magnitude (mag) means that about 68% of the emission from a galaxy at visual wavelengths is lost, while the average for some of the black body radiators of our galaxies is A_V~47 mag. This means that the amount of visual band radiation is completely negligible, and these black body radiators would be almost entirely invisible to spectrometers that measure in visible spectrum. To put the magnitude of A_V in mathematical perspective, it is helpful to note that A_V is directly proportional to τ_v through this proportion:

$$A_V = 1.086\tau_V \tag{2.2}$$

Now that we know how the source of the light is obscured, we must define how we measure the intensity of the source in the first place, before it reaches our observing instrument, and even before it interacts with any particles. We model the source of our infrared electromagnetic radiation as a black body. A black body is defined as an idealized physical body that completely absorbs all electromagnetic radiation that is incident upon it. Consequentially, the black body then reemits this absorbed light in a constant spectrum that is identifiable by its temperature. It is called a "black body" because, if it were to have a temperature of 0 K, it would emit no light at all, and thus would appear to be black. Other important details about the nature of the reemitted light are that the intensity of the light is isotropic, meaning it does not vary with the angle of emission, and that it emits light with just as much energy or with greater energy than any other type of physical body at its defined temperature. Figure (2.2) shows the plotted irradiance of black bodies at various temperatures.

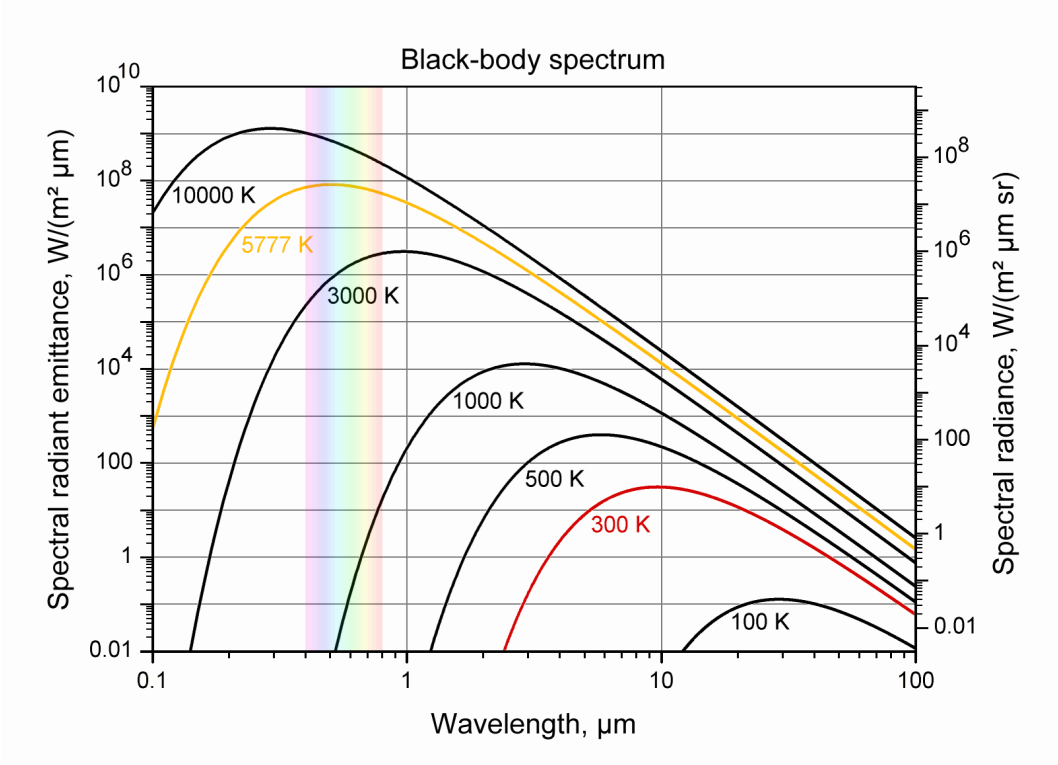

Figure (2.2): The irradiance of black bodies plotted at various temperatures on a logarithmic scale vs wavelength. 300 K is room temperature and it should be noted that black bodies at this temperature have their peak emission in the infrared. 5777 K is the temperature of the sun, and the colored band denotes the range of visible wavelengths, which is important since this is the range of wavelengths visible to most life forms. (http://archive.larouchepac.com/node/15672)

The intensity of the light emitted from any such black body is defined by Planck's Law of black body radiation. Planck's Law is defined as:

$$B_\lambda(\lambda, T) = \frac{2hc^2}{\lambda^5} \frac{1}{e^{\frac{hc}{\lambda k_B T}} - 1} \tag{2.3}$$

Where h is Planck's constant, c is the speed of light, k_B is Boltzmann's constant, λ is the wavelength, and T is the temperature. Using $B_\lambda(\lambda, T)$ as our $I_{\lambda,0}$ in equation (2.2) allows us to calculate the actual intensity of the light received by the spectrometer.

As mentioned previously, we can model much of the carbonaceous dust that obscures these galaxies as black bodies, because they absorb the majority of the light from the galaxies incident upon them and then reemit it most intensely in the infrared. This contrasts distinctly from PAHs, which only absorbs single photons at a time from specific wavelengths before reemitting each photon in the infrared, or silicates which only absorb photons and then scatter them, allowing us only to observe them and identify them by the "missing" flux, known as an absorption feature.

Chapter 3: Polycyclic Aromatic Hydrocarbons

Polycyclic aromatic hydrocarbons (PAH) are a class of highly stable configurations of hydrogen and carbon elements that are prevalent infrared emitting small dust grains for many galaxies. Aromaticity is the theory that electrons involved in the bonds between carbon atoms are free to move cyclically from one carbon atom to another, a process known as delocalization, and that creates alternating single and double bonds between carbon atoms, a process known as resonance. The alternating resonance structures act simultaneously, and thus in essence add extra strong bonds to the already existing strong carbon-carbon bonds. In addition to the aromaticity of PAHs, they are polycyclic as well, meaning that there are many aromatic rings bonded together. Thus, PAHs are unusually stable and are very unlikely to react or change structure naturally.

Another important characteristic to note about PAHs is that they are generally formed in excess as a byproduct of very hot combustion reactions. When carbon fuels are combusted, hydrogen is broken off of the hydrocarbon chains and acetylene, another type of hydrocarbon, takes its place, until the polycyclic aromatic rings begin to form and all of the fuel has become a highly stable PAH. Thus, nearby galaxies that are undergoing or have recently finished a period of active star formation are often densely enshrouded by carbonaceous dust and PAHs, since star formation involves plenty of combustion (Smith et al. 2007)

When PAHs become dense in the interstellar medium (ISM) of a galaxy, they begin to absorb some ultraviolet (UV) and visible light and then reemit it very strongly in the mid infrared (MIR) portion of the infrared spectrum, along with our carbonaceous/silicate dust which emit as blackbodies. Thus they are critical contributors to our observed infrared spectra. Due to the

nature of the excitation of their resonant cyclic aromatic bonds, they emit in spikes at specific wavelengths.

Astrophysically, the features we are most concerned with are at 3.3 μm, 6.2 μm, 7.7 μm, 8.6 μm, 11.2 μm and 12.7 μm, which are the brightest and most well-studied PAH features. Each of these features corresponds to a different way that the bonds of the PAHs are excited. The 3.3 μm emission happens when the C-H is stretched; at 6.2 and 7.7 μm, the C-C is being stretched; the 8.6 μm feature is caused by an in-plane C-H bend; and the 11.2 μm and 12.7 μm emission happens when an out-of-plane C-H bend occurs (Draine 2001). Each of these stretches and bends occurs when a PAH structure absorbs a far ultraviolet (UV) photon, and the varying strength of each of these features is attributed to the ratio of singly positively charged PAH particles, known as cations, to neutrally charged PAH particles (Omont 2007).

We are interested in the strength and prevalence of these PAH features in the spectra of our galaxies because they provide important indicators as to some of the characteristics of the galaxies themselves. It is thus important to note why strong PAH emission occurs, as well as why weak or no PAH emission occurs: When there is a large presence of PAH emission in a spectra, it can be concluded, as mentioned before, that the target galaxy is currently undergoing, or has recently undergone, an intense period of star formation, and thus has produced a lot of PAH particles as byproducts of the intense combustion, as well as excited these PAH particles with UV radiation. This means that the galaxy is very likely to be dominated by starburst regions (Smith et al. 2007; Omont 2007). On the other hand, a lack of PAH emission compared to the dust continuum, thus indicating a deficit of PAH or PAH extinction in the ISM, occurs when the galaxy's active galactic nuclei (AGN), or a galaxy with an actively accreting super massive black hole, has destroyed these PAH particles with its high energy radiation. Therefore,

weak PAH emission is oftentimes potentially linked to galaxies that are dominated by AGNs (Smith et al. 2007; Omont 2007).

In our fitting, we use two of the four PAH flux templates found in Smith et al. 2007 to model the PAH emission for our various galaxies. Figure (3.1) plots each of these templates. These PAH templates were modeled by fitting the continua and PAH emission of heavily PAH dominated galaxies, averaging their infrared spectra in groups defined by certain physical parameters, and then modeling the averages using the model originally used to fit the source PAH spectra. The model used to fit the PAH spectra includes a galaxy's the continuum of starlight and the thermal dust continuum, as well as emission due to dust and H_2 (Smith et al. 2007). The specifics of these fitting features are discussed in greater detail in Smith et al. 2007, but it should also be noted that the fitting method here also uses the Levenberg-Marquardt method to solve a non-linear least squares problem, very similar to the way we fit the spectra of our own galaxies. In addition, it is important to note that the dust features are modelled using a series of blended Drude profiles, which are discussed in greater detail below (Smith et al. 2007).

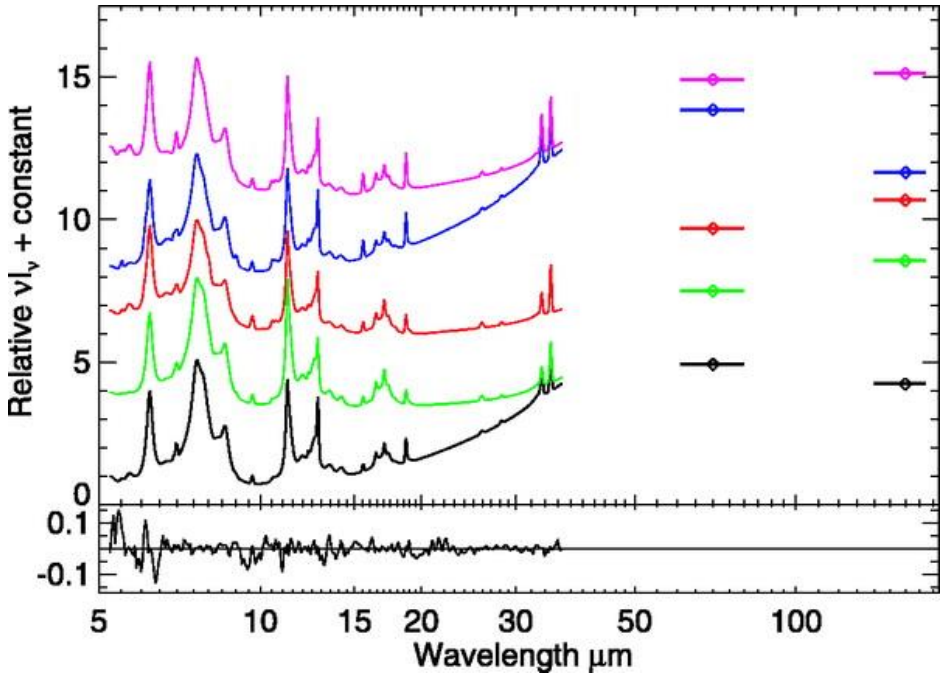

Figure (3.1): Each of the PAH templates from Smith et al. 2007. Note that these templates include black body emission and extinction of the emission of each PAH feature. Our figures are refitted for pure PAH emission.

In order to implement these PAH templates into our own fits, we use the original software that fit the PAH templates, PAHFIT, to refit the templates. This provides us with a model of the PAH emission that we can analyze to recover the strengths of its emission features. The model equation we use to refit these PAH features is as follows:

$$I_\nu = \frac{(1 - e^{-\tau_\lambda})}{\tau_\lambda} \sum_{r=1}^{R} I_r(\nu) \tag{3.1}$$

where τ_λ is the optical depth, $I_r(\nu)$ is each fitted, unextincted Drude profile with a unique set of fitted parameters, and R is the number of fitted Drude profiles. It is important to note that here we use mixed extinction, as opposed to the screened extinction used for fitting black bodies, with the major difference being that the absorbing particles are modelled as being mixed in with the emitting sources, as opposed to being treated as a foreground screen through which all of the

emission is viewed. Figure (3.2) shows an estimate of a single Drude profile. The equation we use for each Drude profile is:

$$I_r(v) = \frac{b_r \gamma_r^2}{\left(\frac{\lambda}{\lambda_r} - \frac{\lambda_r}{\lambda}\right)^2 + \gamma_r^2} \tag{3.2}$$

b_r is the central intensity, γ_r is the fractional full width half max (FWHM), and λ_r is the central wavelength, which is where b_r occurs (Smith et al. 2007). This becomes evident when one calculates $I_r(\lambda_r)$ and the equation yields b_r . The units of $I_r(v)$ are watts per meters squared per Hz (W/m^2Hz). Drude profiles are very similar to Lorentzians in that they have most of their power in their extended wings. When the wings of multiple Drude profiles overlap, they can become the highest contributing factor to a continuum, and they often do in certain PAH dominated galactic spectra (Smith et al. 2007). The integrated intensity of the Drude profile comes from Smith et al. 2007 as well:

$$I_r \equiv \int I_r(v) dv = \frac{\pi c}{2} \frac{b_r \gamma_r}{\lambda_r} \tag{3.3}$$

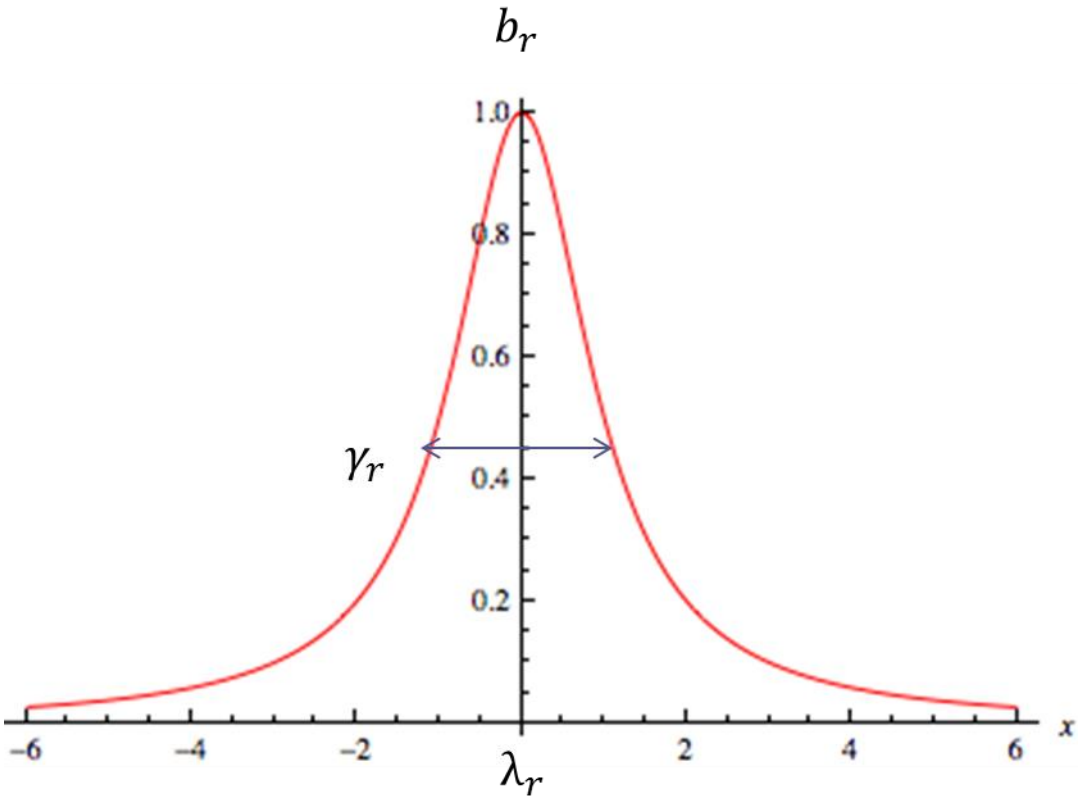

Figure (3.2): A Lorentzian profile, which is almost identical to the Drude profiles we use. b_r is the central intensity, λ_r is the central wavelength, and γ_r is the fractional full width half max. Most of the profiles' power comes in the extended wings, which is unlike a Gaussian, which has most of its power in its central bell curve.
(http://mathworld.wolfram.com/LorentzianFunction.html)

Nevertheless, the most useful means of measuring the strength of PAH emission features is via measuring the equivalent width of one of the Drude profiles of interest that is a part of the PAH profile. Sometimes, absolute intensity is not as useful as it should be when comparing the intensity of one spectral line feature to another due to extenuating circumstances. Thus, it is often times more helpful to observe the relative intensity of a line feature with respect to the continuum it contributes to. Thus, the equivalent width of a line feature is the area between the spectral line itself and the continuum it is related to, with the continuum normalized to one.

Thus, this provides a comparable relative intensity of one line feature to another, which is much more helpful when their absolute intensities may prove to be misleading. It is called the "equivalent width" because the calculated area is then modelled as a rectangle with a height of 1 below the continuum, which has been normalized to 1, and a width that reconstructs the area calculated from the spectral line. Figure (3.3) is a graphic of the mechanism of how equivalent width functions.

Mathematically, we define the equivalent width by:

$$W_\lambda = \int_{\lambda_1}^{\lambda_2} 1 - \frac{I_{\lambda,0}}{I_\lambda} d\lambda \tag{3.4}$$

$I_{\lambda,0}$ is the continuum level without the effects of the spectral line, and I_λ is the measured relative intensity of the line feature with respect to the continuum. Equivalent width is measured in units of wavelength, such as angstroms or microns. Since the height of the rectangle is normalized to be 1, W_λ is equivalent to the entire area of the rectangle.

The reason that equivalent width is relevant to PAH features is that the pure emission of the various PAH features are hard to compare, given that certain ones happen to occur in places where the entire continuum happened to be brighter than somewhere where a different PAH feature occurred. Thus, if the entire continuum is normalized first, it easier to see just how intense the feature is by itself, without the effects of the black bodies, silicate, or water ice absorption that all affect the continuum itself.

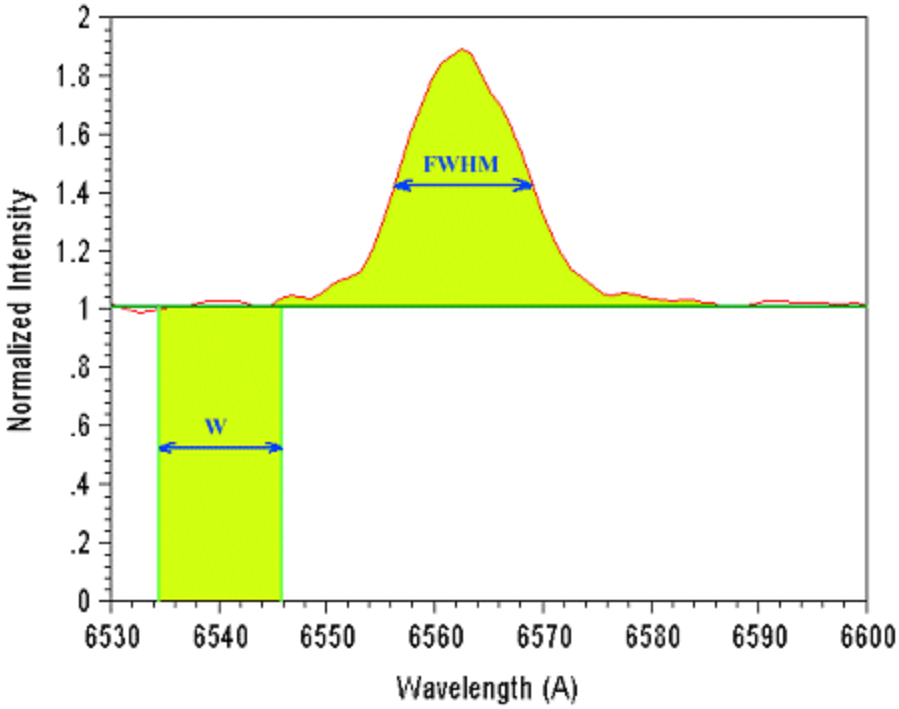

Figure (3.3): A plot of a line feature relative to its normalized continuum, as well as its equivalent width. FWHM demonstrates the width of the full width half max. As can be seen, the height of the rectangle is 1, and thus, the intensity of the spectral line is completely measured by W, the equivalent width. This makes comparing the intensities of various line features much simpler. (http://www.astrosurf.com/buil/us/spe2/hresol7.htm)

Chapter 4: Fitting the Spectra

With any given set of source data, it is often a useful exercise to create a model that most closely resembles the source data, but, unlike the source data, is described by an equation that can be manipulated and can undergo more efficient statistical analysis. Frequently in physics and other sciences, a linear fit is used in order to quantify the correlation of the raw data to the linear relation that is proposed to describe it. However, in our fitting process we are making a non-linear fit in order to solve a least squares problem. What this means is that we take an initial general "guess" at what a fit might look like for any given spectra, test how closely the fit resembles the raw data, and then adjust the fit parameters to resemble the data more closely. The test we use is a chi-squared (χ^2) test, which gives a numerical estimate without units of how close the fit is to the data by roughly taking the difference between the fit and the model, squaring it and then dividing by the errors. As soon as further adjustments on the fit no longer show a statistically significant improvement on the fit, the fitting process is complete. The method described above is a summary of the Levenberg-Marquardt technique.

All of this means that we are attempting to choose the physical parameters that were most likely to have occurred in order to produce the observed flux. The physical parameters we are most interested in testing, as mentioned previously, are black body temperatures, visual extinction coefficients, τ peak of the absorption features, PAH fluxes, and PAH equivalent widths. In beginning this process, we can choose an initial value for each of these, along with the normalization factor, and allow it to be adjusted according to the fit, or fix it if we believe a preset parameter will be required to produce a physically realistic result. These initial values are used to begin the fitting process using a visually extincted model of a black body using Planck's law. From here, the initially provided parameters are adjusted to reduce the χ^2 value of the

model. χ^2 here tells us the likelihood that the 2 or 3 black bodies, along with whichever PAH template may come into play, would have produced the given source flux of the spectra. The degree to which each of these parameters is adjusted is steadily decreased through each iteration until the reduction in the χ^2 value is no longer significant. Finally, the fitted black bodies and PAH emissions are summed up and the fit is plotted. Since we fit each curve twice, once per each extinction curve, we then compare both fits visually to determine the best one.

The following is the equation we use to quantitatively determine the χ^2 of each fit:

$$\chi^2 = \sum_{\lambda} \left[\frac{F_{obs(\lambda)} - F_{mod(\lambda)}}{Err(\lambda)} \right]^2 \tag{4.1}$$

Where $F_{obs(\lambda)}$ is the observed spectra from CASSIS, $F_{mod(\lambda)}$ is the model function we use, and $Err(\lambda)$ is our error function. The whole equation is indexed by wavelength. $F_{mod(\lambda)}$ is defined as:

$$F_{mod}(\lambda) = \sum_{i=1}^{N_B} a_i \frac{B_{\lambda,i}(\lambda, T_i) e^{-\tau_{\lambda,i}}}{\max(B_{\lambda,i})} + \sum_{i=1}^{N_{PAH}} b_i \frac{F_i^{PAH}(\lambda)}{\max(F_i^{PAH})} \tag{4.2}$$

For the left hand summation, N_B is the number of fitted black bodies, $B_{\lambda,i}(\lambda, T_i)$ is the Planck's law of blackbody radiation, $e^{-\tau_{\lambda,i}}$ is our extinction factor, $\tau_{\lambda,i}$ is our optical depth for the black body, and a_i is the normalization factor. For the right hand summation, N_{PAH} is the number of PAH templates, $F_i^{PAH}(\lambda)$ is the flux of the template, and b_i is the normalization factor. We normalize both by dividing by the maximum value and fitting the respective normalization factors to each point in order to prevent large variations in the model output.

The $Err(\lambda)$ function requires some further explanation: normally, error is just the 1 standard deviation (σ) of $F_{obs(\lambda)}$, but our $Err(\lambda)$ has another factor as well. Part of how we define our error function includes fitting the source spectrum using power-laws, which is, in

brief, a parameter that is used in the calculation of luminosity distributions of galaxies (Schweitzer et al. 2008). This portion of the function is defined by:

$$Err(\lambda) = \frac{F_{PL}(\lambda)}{\sqrt{\Delta\lambda/\lambda}} \tag{4.3}$$

Where $F_{PL}(\lambda)$ is the power law fit and $\Delta\lambda$ is the sampling density of various ranges of wavelengths, which is measured in micrometers (Schweitzer et al. 2008). In addition to this detail, because certain wavelength regions have better sampling than others, we calculate this portion of the error as inversely proportional to the square root of $\Delta\lambda$, so that the aforementioned regions do not dominate the fit just because their sampling happens to be finer than others (Schweitzer et al. 2008).

We found that our fits are most accurate when weighting our model with an average of the power law fitted error and the error based on $F_{obs(\lambda)}$, and thus, this is what we use to weight our model in all cases.

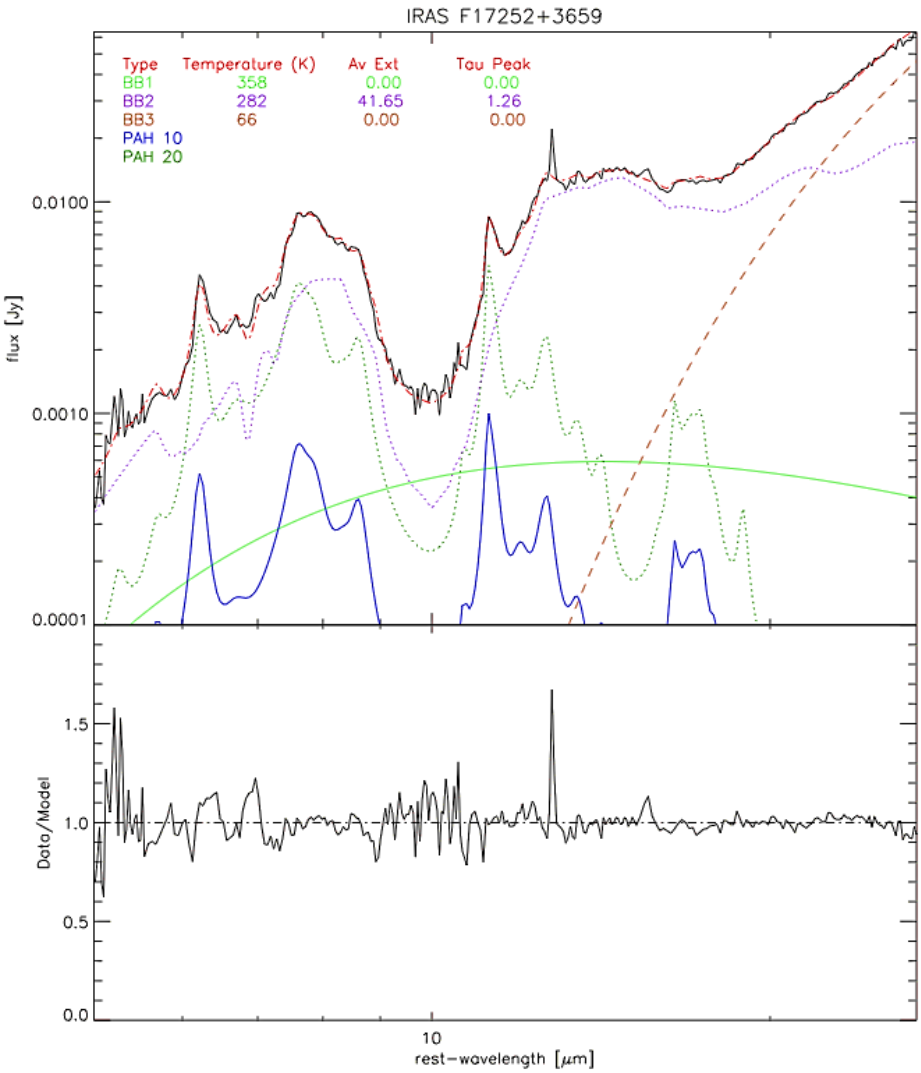

Figure (4.1): Example fit of galaxy IRAS F17252+3659. The light green is the hot black body, the purple is the warm black body, and the brown is the cold black body. Blue is one PAH template and dark green is the other. The graph underneath is the residual. It is important to note that, due to the exponential nature of both the extinction and the emission from the black bodies, we plot both emission and absorption features on a logarithmic scale. Finally, it is also important to note that we do not fit emission lines in our fits. We skip over these points, and thus we do not attempt to extract or record their fluxes.

We used the Information Data Language (IDL) software package QUESTFIT to fit the spectra. QUESTFIT begins by creating a model function to supply to MPFIT in order to begin the fitting process. MPFIT is an IDL software package designed to solve least square problems

by reducing a functions χ^2 value via the Levenberg-Marquardt technique. For our fits, we supply three, and in special cases two, black bodies that are visually extincted to MPFIT, along with instructions as to which parameters are allowed to be adjusted to reduce the χ^2 value of the fit. MPFIT then returns the adjusted parameters that are best suited in solving the least squares problem. QUESTFIT then uses these parameters to construct the proper black bodies, along with PAH emissions determined by PAHFIT, and sums and plots the fit according to the returned parameters.

In terms of what can be expected of adjusted fit parameters, the hot and warm black bodies are often heavily extincted to account for the heavy silicate absorption from 8 to 12 μm and also to account for the more shallow silicate absorption feature from about 14 to 18 μm. Additionally, the hot and warm black bodies can often be absorbed from 4 to 8 μm due to water ice and hydrocarbon absorption. The cold black body produces little emission at these wavelengths, and thus is less extincted here than at the wavelengths at which it peaks.

We used two different silicate absorption profiles to fit the spectra, but both were applied as screened extinction. Figure (4.2) plots both of these extinction curves. “Screened extinction” means that the medium causing the extinction of the target is viewed as a foreground screen through which the target must be observed, as opposed to mixed extinction, where the target is viewed with the extincting substance mixed in homogenously with the target. Each target was fit with both extinction curves and both of the fits were compared in order to determine the closer fit. Since a significant amount of fits were vastly improved using one extinction curve over another, it was justifiable to use both. We fit 82 of the spectra with the interstellar silicate absorption features modelled in Chiar et al. 2006. In this work, the two silicate profiles are constructed by using the silicate profiles of WR 98a (representing the local ISM) and GCS 3

(representing the Galactic center), as well as from other notable near-IR extinction measurements in the 1.25 to 25 μm range (Chiar et al. 2006). We fit the other 117 spectra using an extinction curve based off of the galaxy IRAS F0857+3915. The two curves are similar, but the curve from Chiar et al. 2006 is more heavily extincted at the deepest silicate absorption from 8 to 12 μm and the range of the second peak for both are offset slightly from each other.

These extinction curves include, as mentioned previously, heavy silicate absorption features. Silicates absorb most strongly when their Si-O bonds stretch, which causes the deepest absorption resonances around 10 μm (Draine 2003). Additionally, there is a not quite as strong absorption feature at 18 μm due to O-Si-O bonds stretching (Draine 2003). While silicates can be either amorphous or crystalline in structure, the absorption features found in the spectra of the galaxies of interest are modeled best by amorphous silicate absorption, since there appears to be no clear structure that can be determined by the featureless absorption features found in our spectra (Draine 2003). The origin of the abundance of silicate in the ISM is hypothesized to be from asymptotic giant branch stars, which are a class of evolving stars that are low to medium in mass. These particular stars are also thought to be oxygen rich and currently losing some of their mass (Chiar 2006).

However, our smoothly varying extinction curve does not only contain silicate dust grains, but also frequently has graphite dust grains included as well. When both grains are modeled with power-law components, the extinction curve was more accurate as long as the minimum of each distribution was $a_{-} \approx 50$ Å and the maximum was $a_{+} \approx 2500$Å. When the dust grains are small, they are assumed to be the PAH molecules we discussed in sections prior, and when they are large they are modelled as more similar to graphite and having properties like it when the particles are larger than ~ 0.01 μm (Draine 2003).

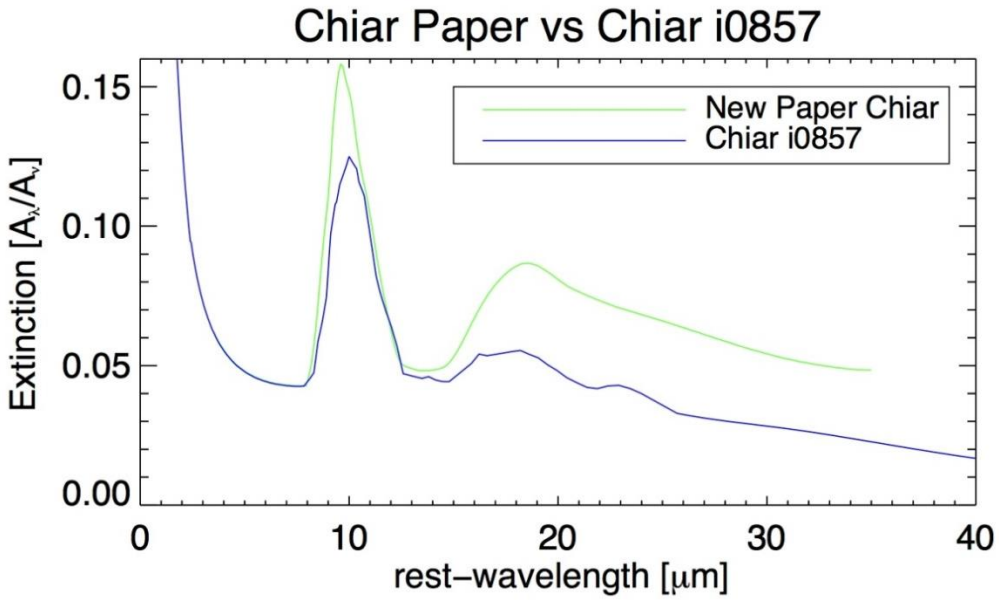

Figure (4.2): A comparison plot of both the extinction curve from Chiar et al. 2006 and the extinction curve based on the galaxy IRAS F0857+3915. The green corresponds to the first and the blue corresponds to the latter. Both the 10 μm feature and the 18 μm feature are deeper for the curve from Chiar et al. 2006. The units of the extinction that is plotted are A_λ/A_V.

Chapter 5: Results and Statistical Analysis

In total, we fit 199 spectra, using interstellar silicate absorption features modelled in Chiar et al. 2006 to fit 82 of them, and using an extinction curve based off of the galaxy IRAS F0857+3915 for the other 117. It was important that we used both of these, because some fits were remarkably better from using one extinction curve over the other. Figure (5.1) demonstrates one of these cases. It is clearly visible where the fit quality suffers from one extinction curve to the other.

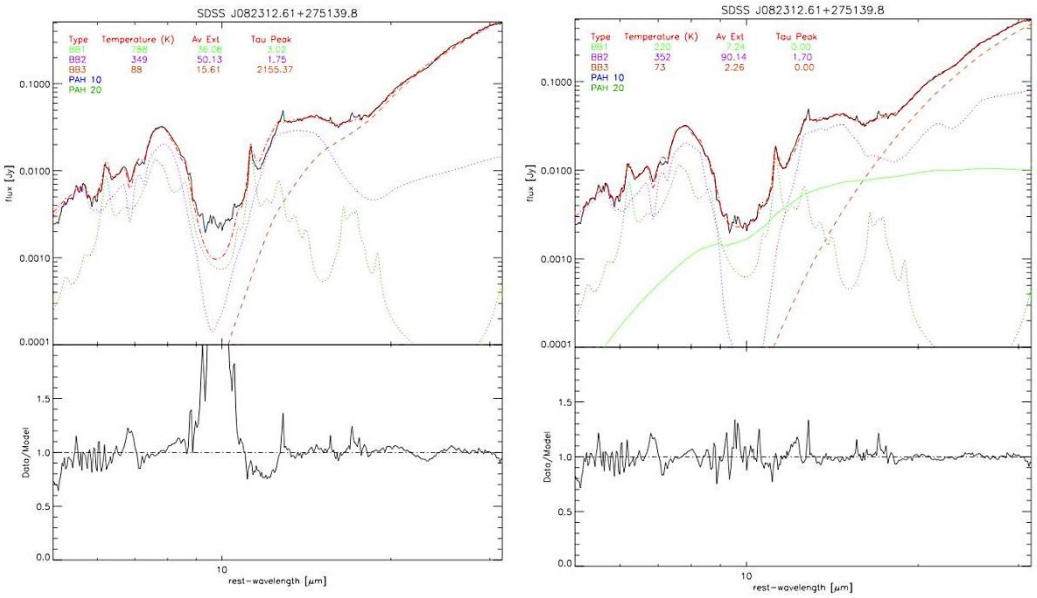

Figure (5.1): Left: Fit using extinction curve from Chiar et al. 2006. Right: Fit using extinction curve based on IRAS F0857+3915. Comparison of two fits to the spectrum of the galaxy SDSS J082312.61+275139.8. At the deep ~9.5 μm silicate absorption feature, the left fit is highly inaccurate, whereas the right fit handles this feature much better. Additionally, at ~12 μm, there is another pretty noticeable deviation from the data by the model. This comparison, and many others showed us that it was beneficial to consider fitting with which ever extinction curve produced a higher quality fit or a more physical fit.

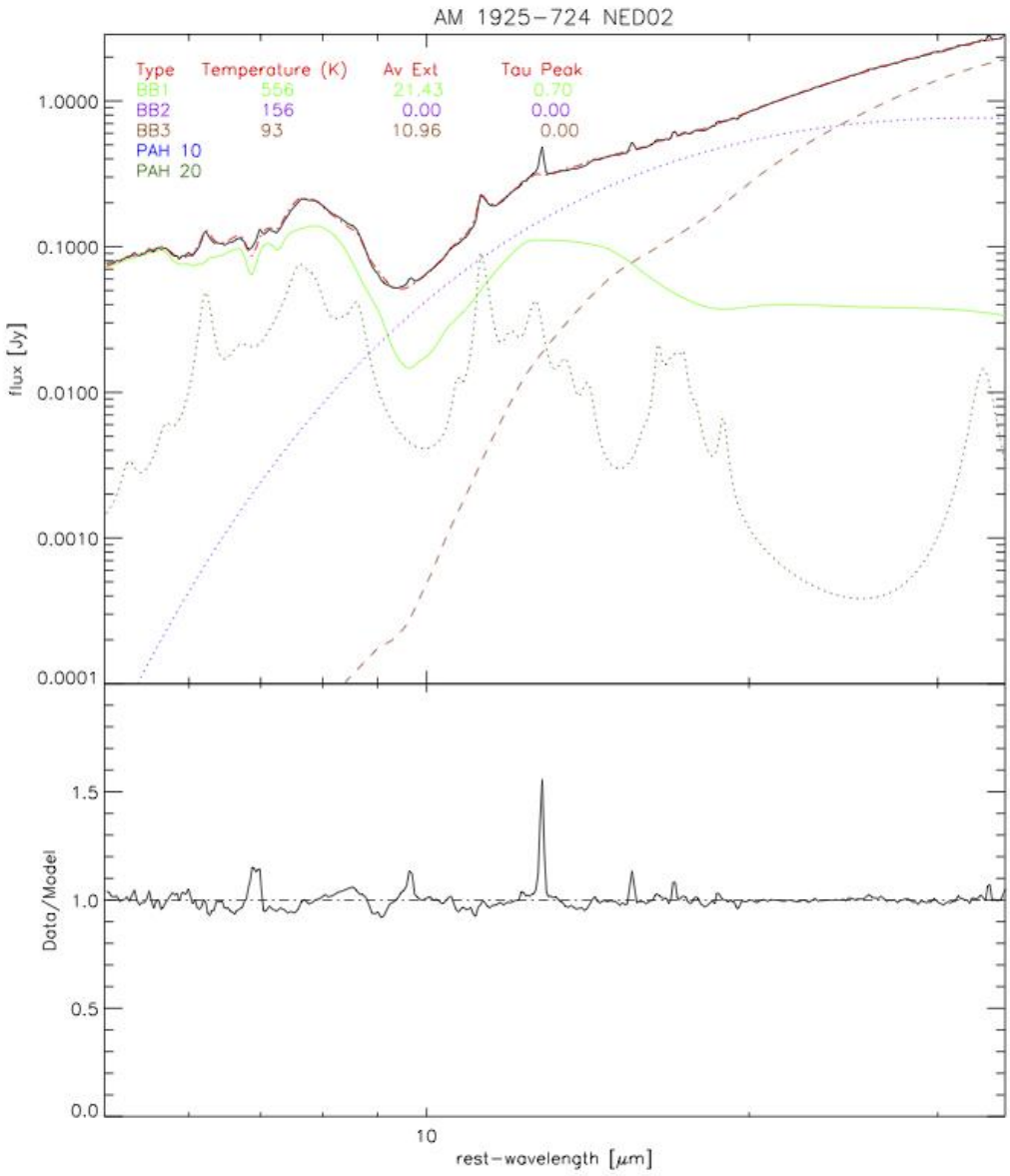

Figure (5.2): This is a fit of the galaxy AM 1925-724 NED02 using the extinction curve from Chiar et al. 2006. This is rather low overall silicate absorption in comparison to the rest of our fits. The water ice absorption is pretty minimal as well. The contribution of the PAH emission seems minimal as well. The noise in the data is completely negligible, and possibly nonexistent. Overall, this is a basic fit that nicely shows the contribution of each black body and some PAH emission.

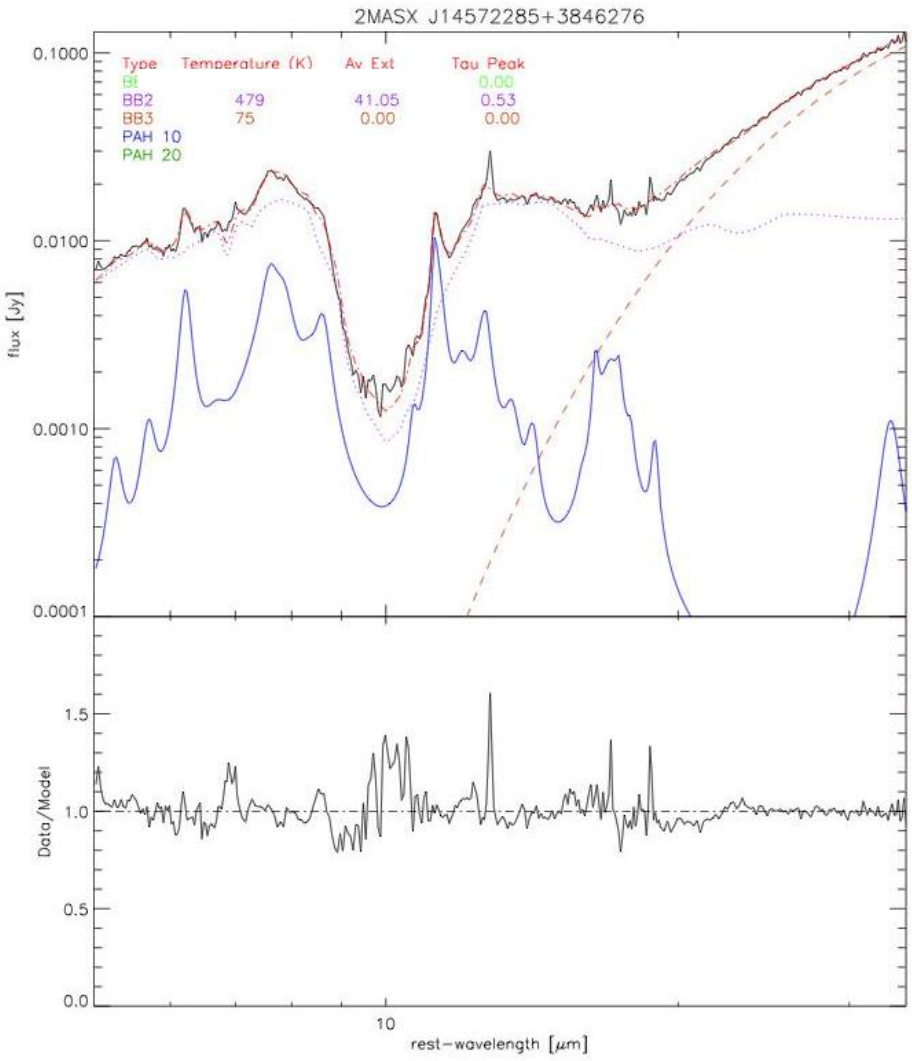

Figure (5.3): A fit of the galaxy 2MASX J14572285+3846376 using the IRAS F0857+3915 extinction curve. This is a good example of a fit with a fair bit of noise, and medium silicate absorption (A_V~41), but with almost no water ice absorption (τ~0.5). Note that this is a good example of a fit with only 2 black bodies as well. Fit also has strong PAH emission features. Also note the strong emission line at ~13.5 μm in the data that we ignore in our fit, because we do not fit emission lines.

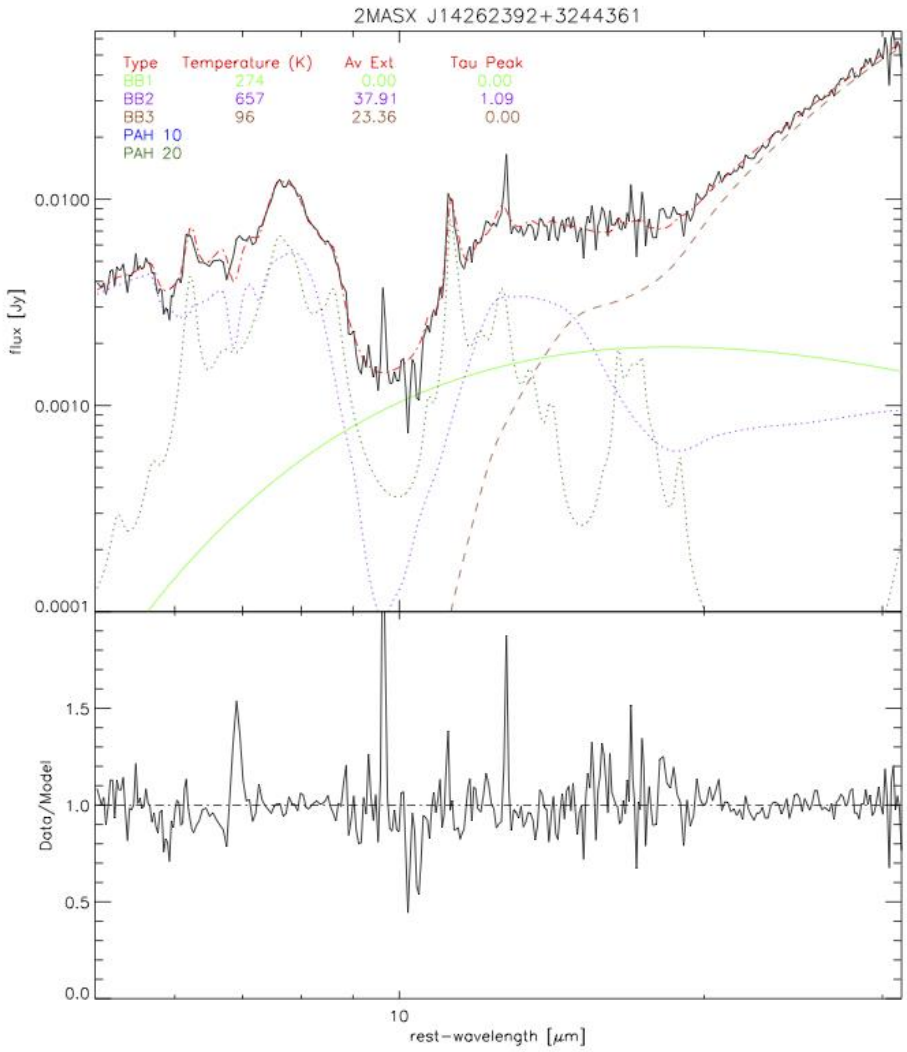

Figure (5.4): Fitted spectrum of the galaxy 2MASX J14262392+3244361. The silicate features from Chiar et al. 2006 were used. While this is a three black body fit, it is notable here that the hot black body and the cold black body are both much more heavily extincted than the warm, unlike the fit above. As one can observe from the distribution of strengths of silicate extinction below, this is a rare case with warm black bodies only having A_V=0 about 4% of the time, whereas hot and cold blackbodies have having A_V=0 about 43% and 35% of the time respectively. An additional detail to note is that this fit has many more absorption and emission lines than in some other fits.

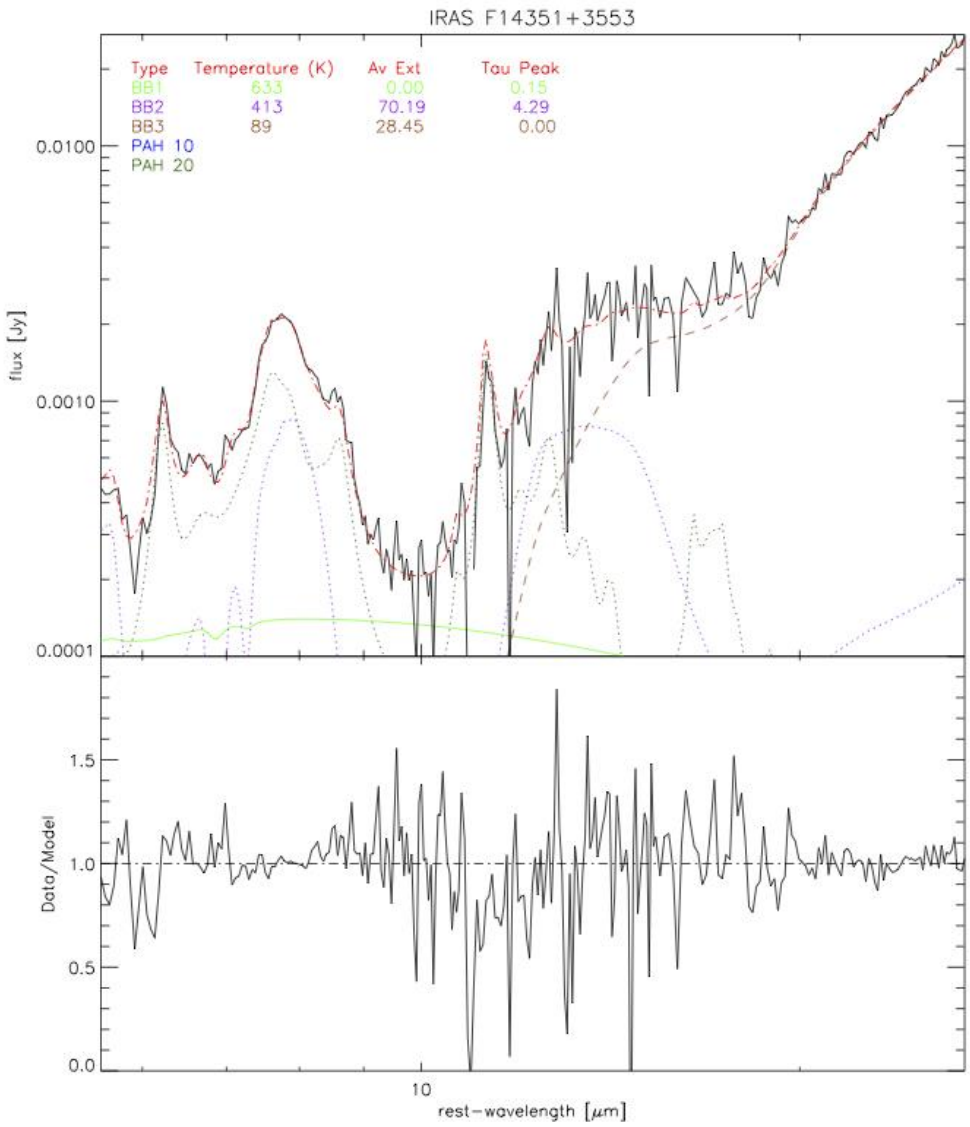

Figure (5.5): A fit of the galaxy IRAS F14351+3553 using the extinction curve from Chiar et al. 2006. This fit has a significant amount of noise, as well as a high amount of silicate and water ice absorption. The temperatures for the hot and warm black body are about a hundred degrees above their average as well. Despite all of these obstacles, the fit quality is still very high, showing the robustness of our fitting technique.

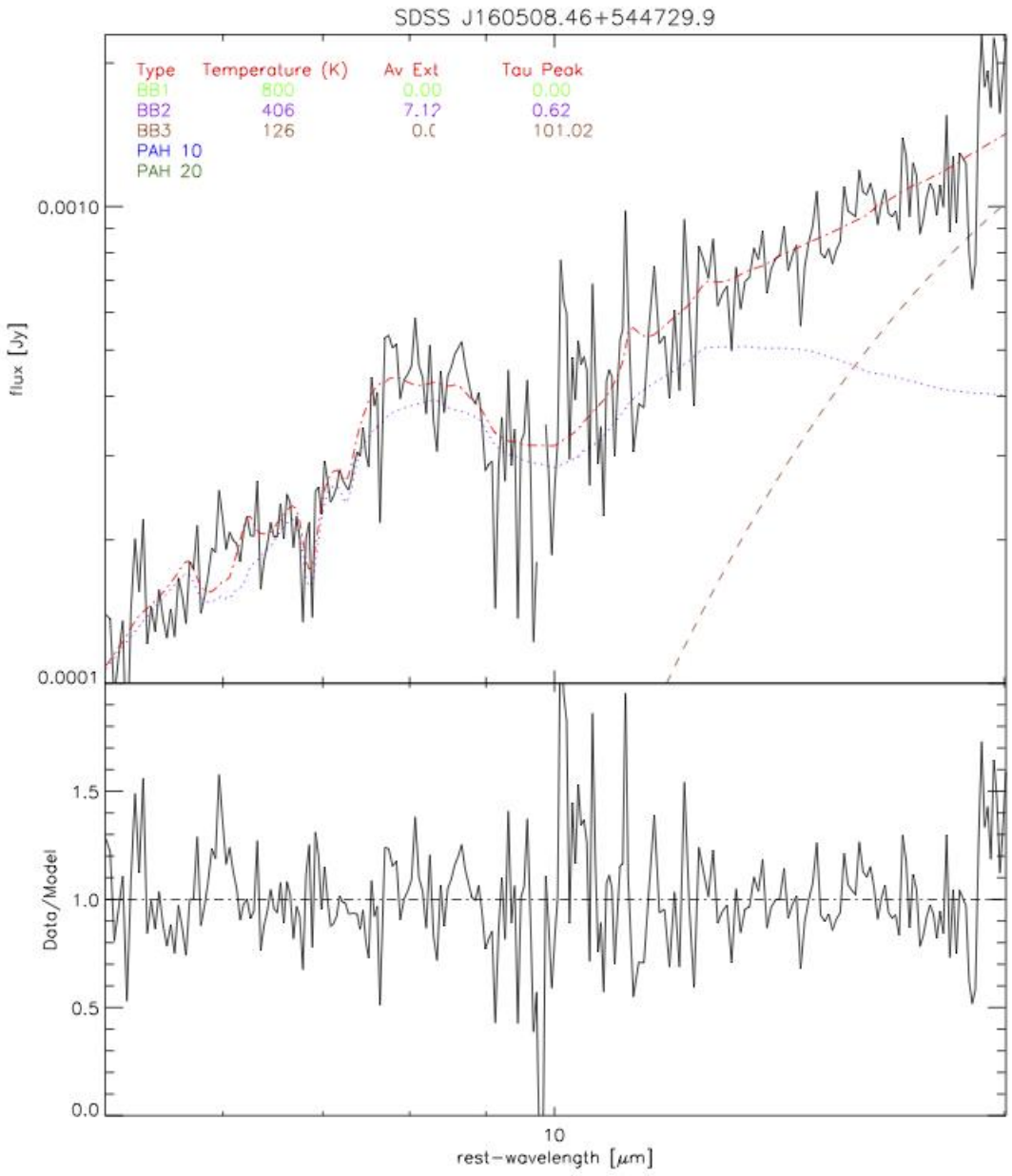

Figure (5.6): The fitted spectrum of the galaxy SDSS J160508.46+544729.9 using the extinction curve based on the galaxy IRAS F0857+3915. The cold absorption is omitted since its effects are negligible. This is among one of the noisiest spectra we fit. Note as well that this is a 2 black body fit, and that most of the noisiest spectra tend to be fit with only 2 black bodies, since it is difficult to parameterize three black bodies as accurately while still dealing with so much noise. That being said, the fit accuracy is remarkable for a spectrum with so much noise. Additionally, and interestingly enough, this fit has one of the lowest silicate absorption intensities as well for all three of the black bodies in total.

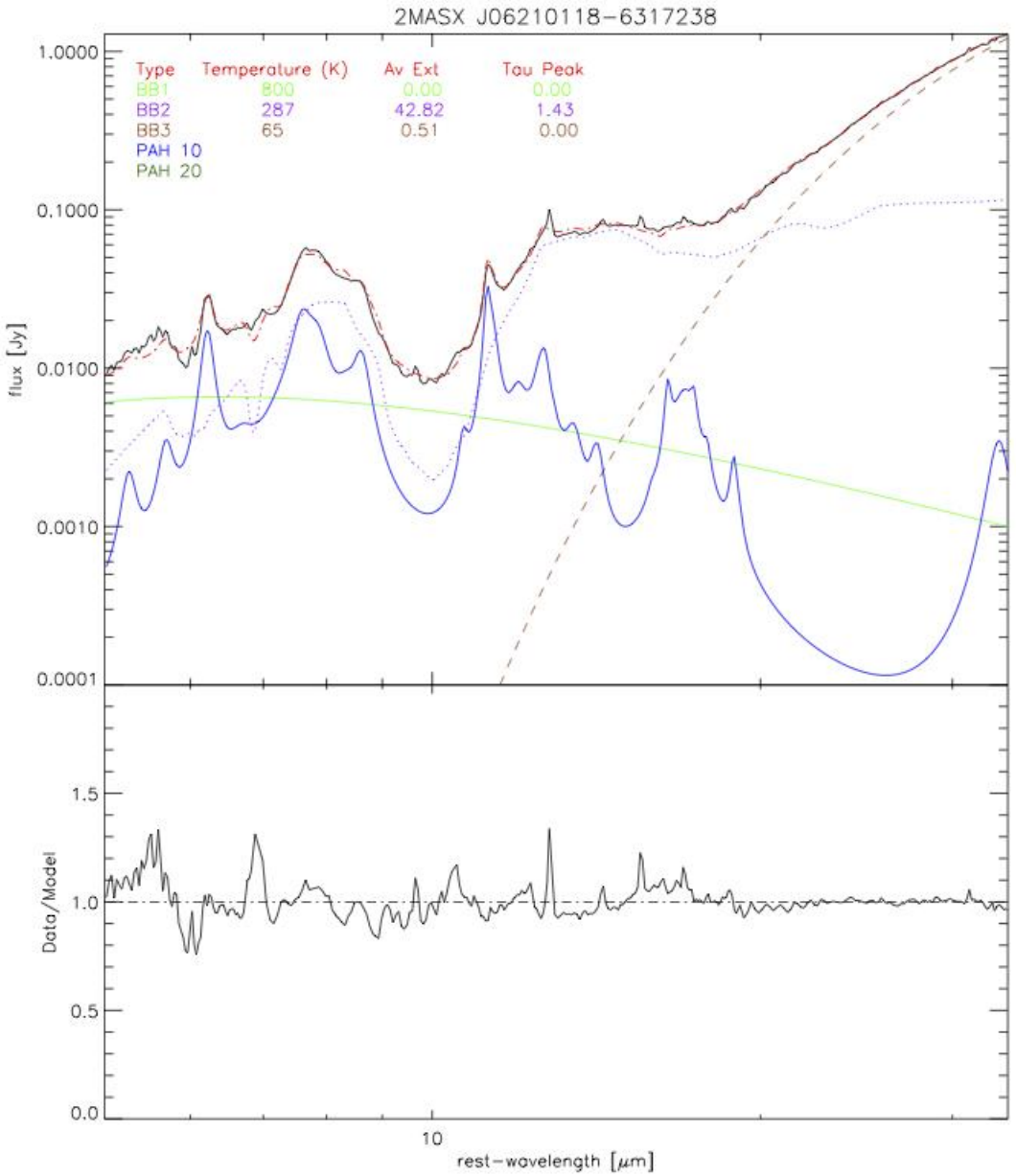

Figure (5.7): Fit of the galaxy 2MASX J06210118-6417238 using the extinction curve from IRAS F0857+3915. While there is nothing particularly remarkable about this fit, it demonstrates a technique we used by which we fixed a hot black body at 800 K to help fit the 9.5 μm silicate absorption feature. This often times was more effective than leaving the hot black body to freely become parameterized. In most cases, we allow all three of the black bodies to be freely adjusted, but we employed this technique when physicality and accuracy of the fit were greatly improved by doing so. The fit above demonstrates one of these cases.

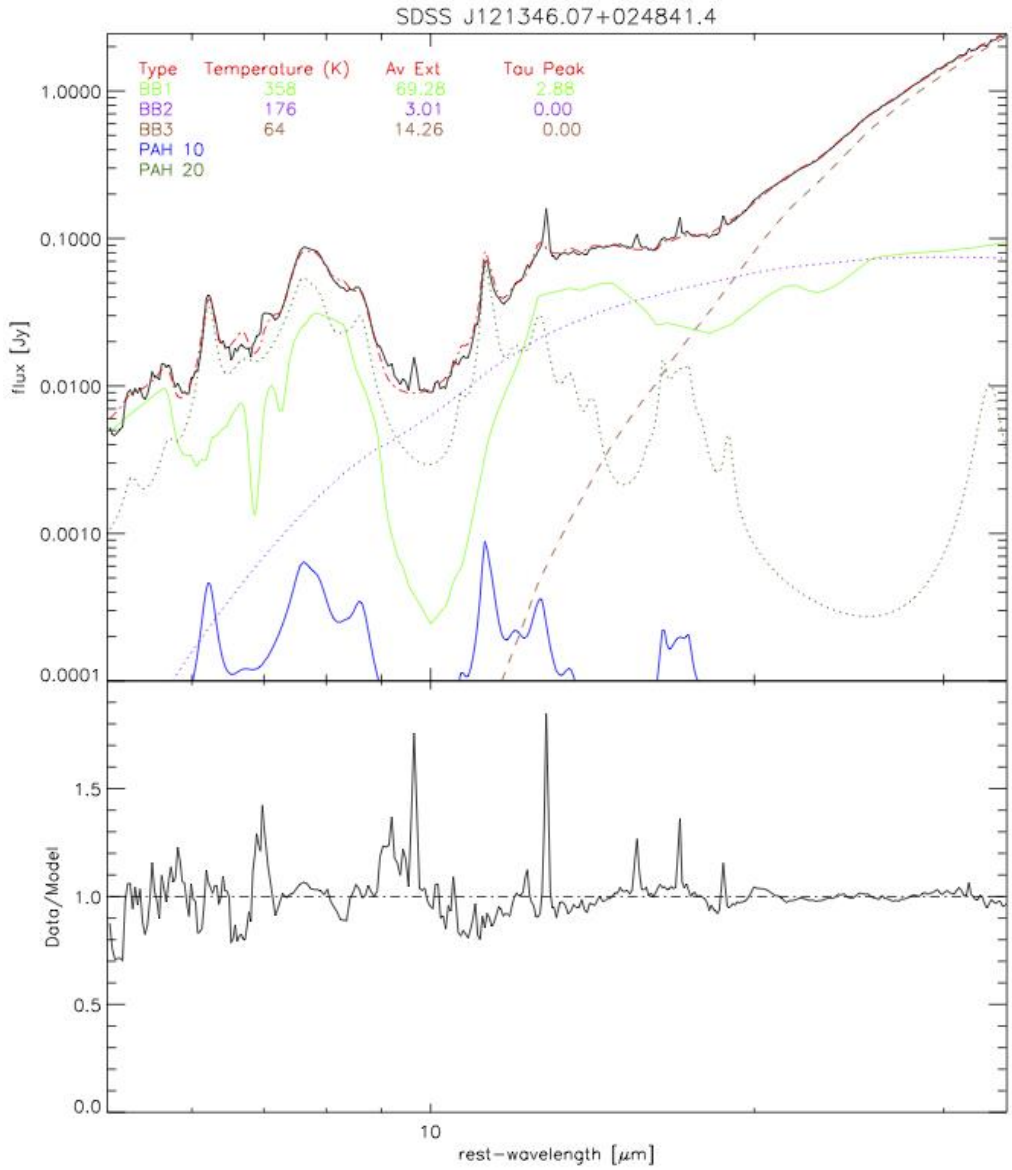

Figure (5.8): A fit of the galaxy SDSS J121346.07+02481.4 using the silicate features from IRAS F0857+3915. This is a unique fit, given that all three of the black bodies are particularly colder than normal, and the hot black body is very heavily extincted as well. $A_V \sim 70$ is far out of reach of $\sigma \sim 1$ for silicate absorption of hot black bodies. Additionally, the warm black body is significantly colder than normal, and looks more like a second cold black body.

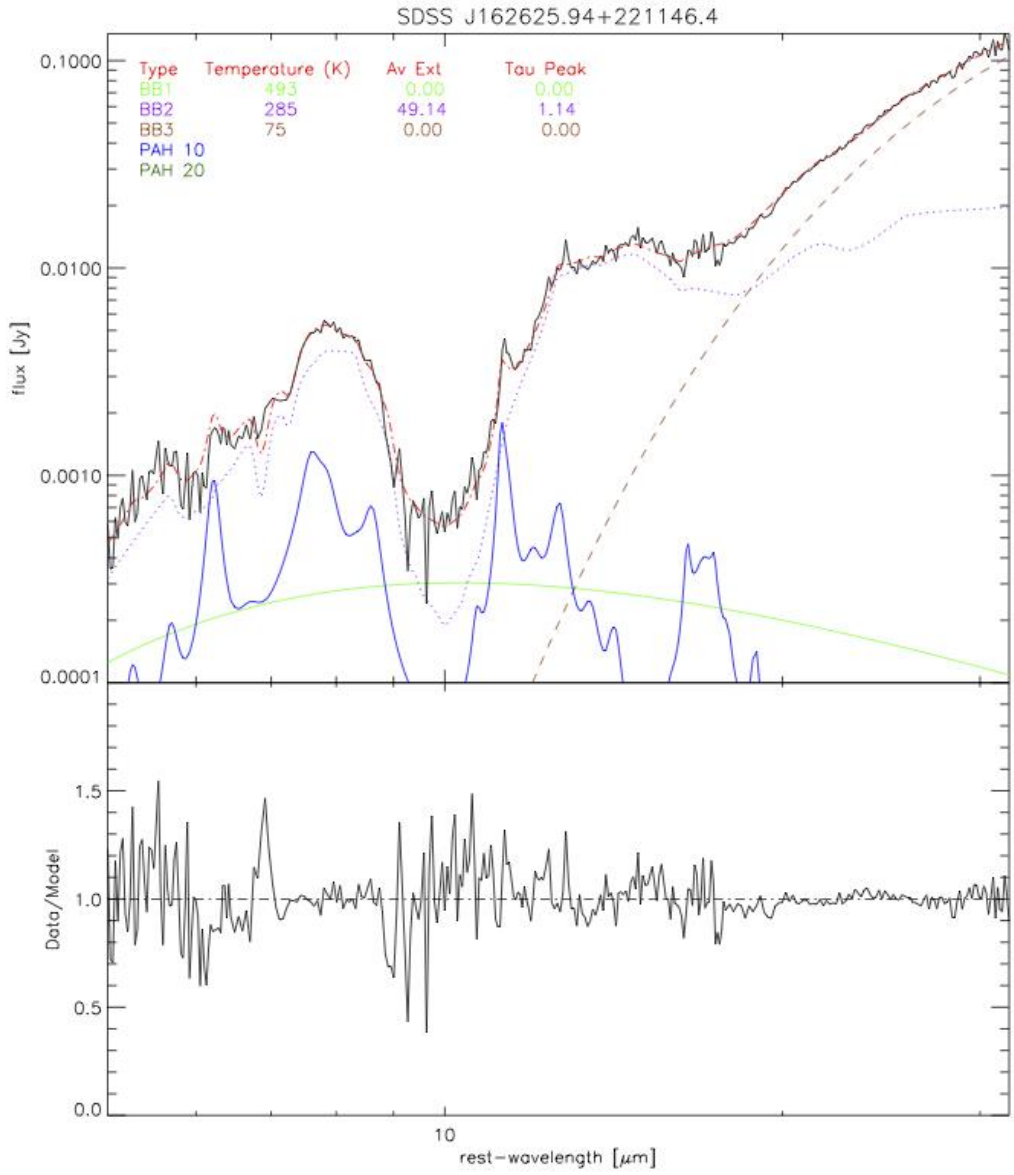

Figure (5.9): Fit of the galaxy SDSS J162625.94+221146.4 using the IRAS F0857+3915 extinction curve. This fit has medium noise and medium silicate and water ice absorption, as evidence by A_V ~50 and τ~1.15. This fit is interesting because both the hot and cold black bodies are fixed, and only the medium black body shows any deviations due to extinction.

As mentioned previously, we extracted the physical parameters describing the fits and organized them for analysis. To reiterate, the extracted observables include the temperatures of

the black bodies, the visual extinction of the black bodies, the amount of absorption due to water ice, and the strength of each PAH emission feature, as well as the equivalent width of each of the major PAH features.

First, it is beneficial to verify that our method of fitting each spectra with either 3 fits (a hot, warm and cold black body) or 2 fits (a hot and cold black body) is in fact a self-consistent model. We can do this by counting how frequently each blackbody was fit at certain temperatures, and comparing their magnitudes relative to one another. Histograms for the temperature of each black body are shown below. The average temperature for the hot black bodies is ~516 K and the median temperature is ~466 K. The mean and median for the warm black bodies are ~319 K and ~310 K respectively. Lastly, the average temperature for cold black bodies is ~83 K and the median temperature for cold black bodies is ~75 K. Thus, our method is self-consistent, since it is clear that, overall, the hottest black body is indeed hotter than the other two black bodies the majority of the time, and the coldest is significantly colder, while the warm black body is somewhere in between. Additionally, the distributions are roughly Gaussian, centered at the average with the majority of the data falling within one standard deviation on either side of the average, which is consistent with the underlying physical parameters being Gaussian.

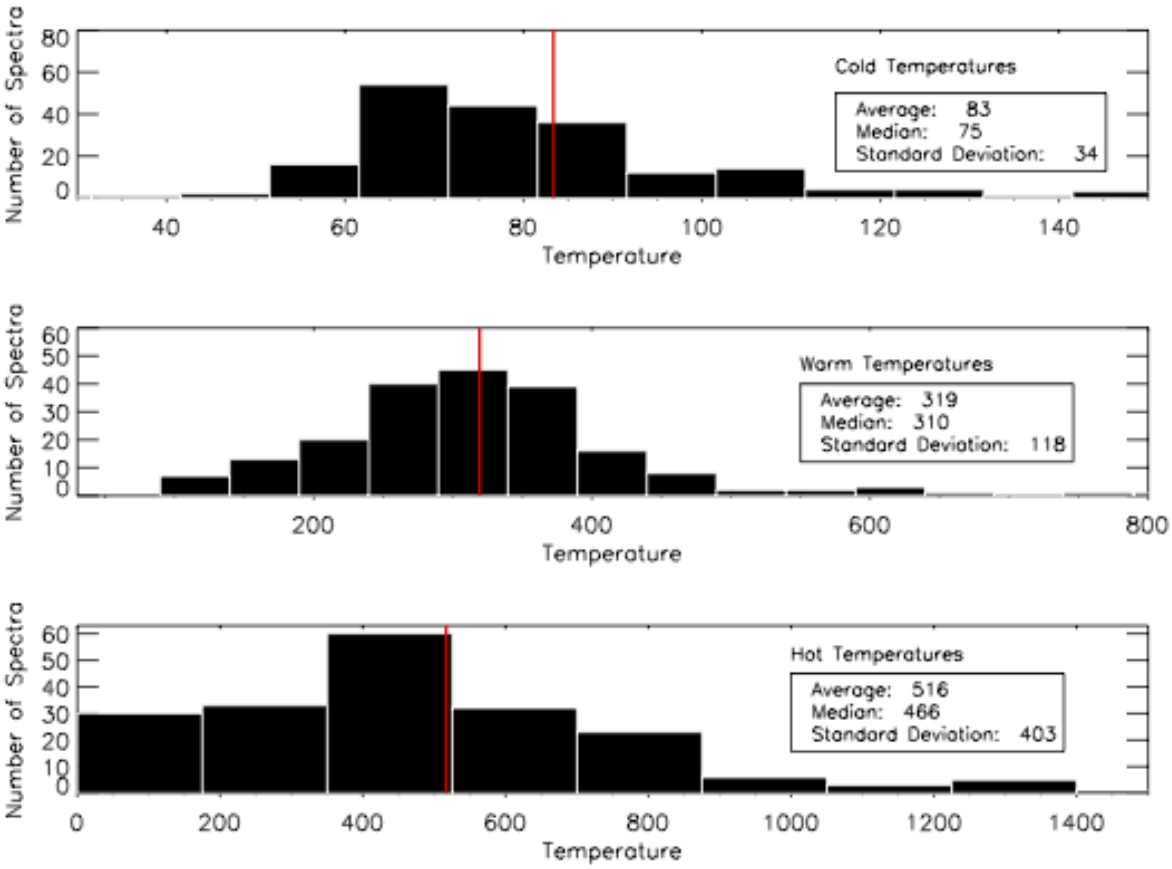

Figure (6.1): Distribution of temperatures of each modelled black body. The red line is average temperature of the group. As can be seen above, most of the data falls within one standard deviation of the average temperature, which means our system is self-consistent for the reasons described above. There is significantly greater deviation between the median and mean of the hot black bodies than the other two because their range of temperatures is so much greater, which is also evidenced by the standard deviation. Some of the hottest black bodies reached temperatures as high as ~2000 K, which are not shown above since there is not a significant amount of these.

In the same vein of validating our fitting procedure, it is also advantageous to statistically verify that the black bodies we are fitting are as visually extincted as we believed them to be, since our entire batch of spectra was chosen because of the intense obscuration of their luminosity at visual wavelengths. Thus, we counted how obscured each fitted black body is per fit in the visual band and plotted the results as histograms, which are again shown below. Indeed, it appears that each of the modelled black bodies for our galaxies is quite heavily extincted the

majority of the time. The median and average visual extinction of our warm black bodies is A_V~47, which is so heavily extincted that only a fraction of a percent of light at visual wavelengths would manage to be observed at all. Additionally, an average of A_V~13 and median of A_V~7 is fairly high for the cold black bodies, as well as an average of A_V~21 for the hot black bodies.

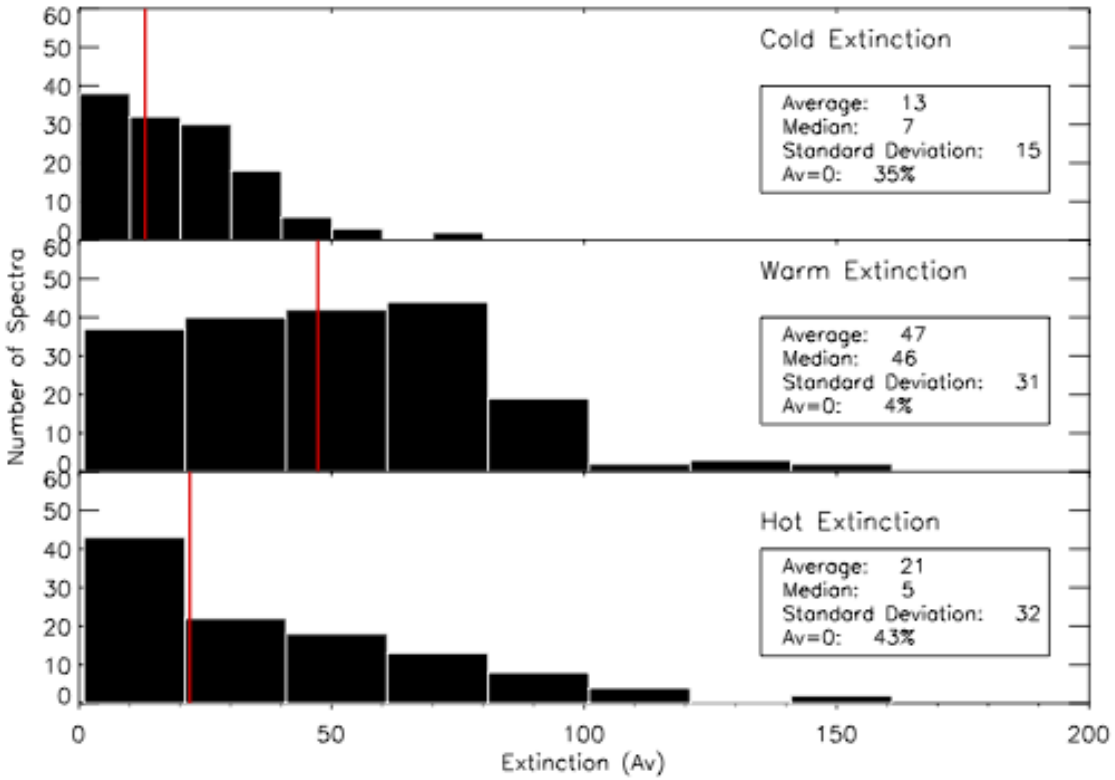

Figure (6.2): Distribution of visual extinction magnitude for each modelled black body. The red line is average extinction of the group. Av~0 is included in the first bin. It is evident above that the warm black bodies are the most heavily extincted due to silicate, as well as the most frequently extincted overall. There is once again the greatest deviation between the mean and the average of the hot black bodies due to their highly dynamic nature. A_V=0 is included in the first bin.

Finally, it is also useful to verify the consistency of our measurements for water ice absorption. Many of the black bodies should in fact be absorbed significantly in the 5-8 μm

range in order to account for the obscuration of some infrared emission due to cold molecular clouds. Thus, we again counted and plotted the how often each warm and hot black body is absorbed at those wavelengths. Cold black bodies are not included because they produce an insignificant amount of emission at the wavelengths of interest, and thus the amount to which they are absorbed is not important. While the magnitude of absorption due to water ice is much lower and not quite as frequent, there is still significant evidence that it is necessary as a fitted parameter.

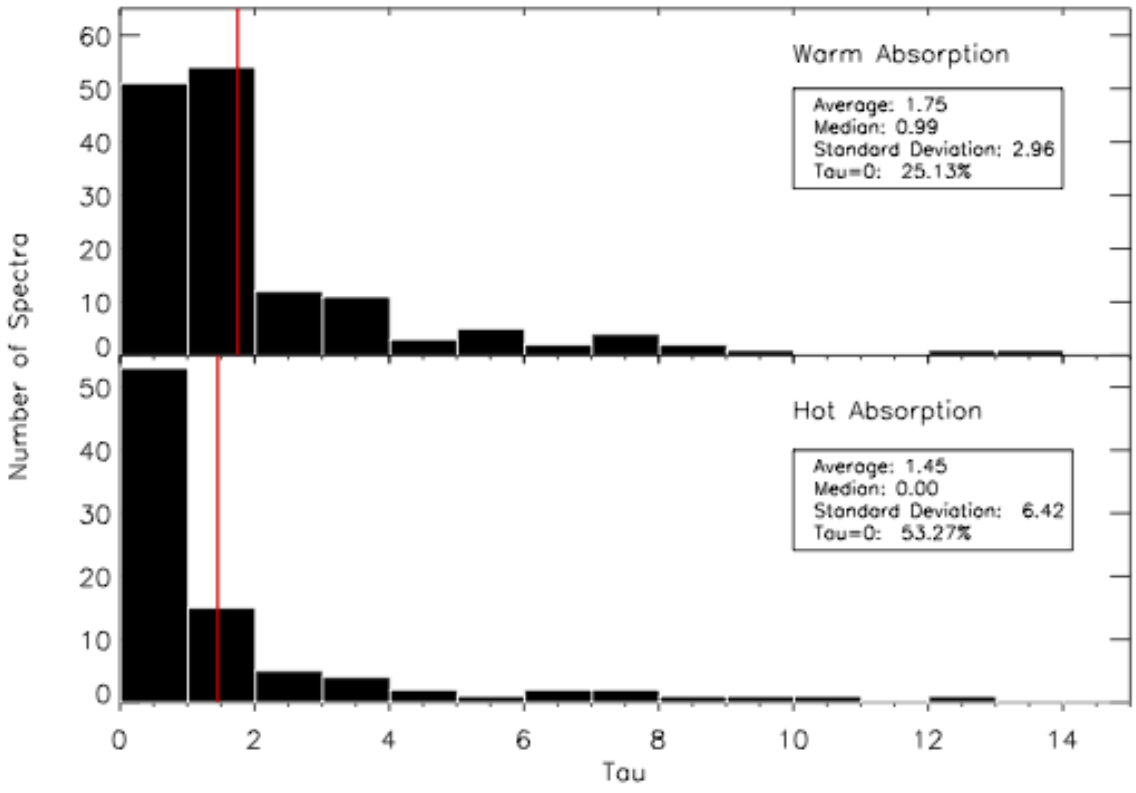

Figure (6.3): Distribution of absorption values for each modelled black body. Red line is average absorption of the group. Cold water ice absorption is omitted because it does not emit significantly enough at the target wave lengths for where this absorption occurs for the intensity of the absorption to be important. $\tau \sim 0$ is included in the first bin.

Chapter 6: Summary and Conclusion

In total, we fit 199 spectra, extracted physical parameters, and analyzed them to verify fit accuracy. In the future, we hope to look at our analyses further in depth to learn more about the nature of the galaxies. Parameters we focused on were the temperatures of the black bodies, the intensity of absorption from silicates and water ice surrounding the black bodies, the emission strength of PAH features and the equivalent widths of some of the PAH features. In our focus on accuracy of fits and physicality of the fits, we found that fitting about three fifths of the spectra with the silicate dust absorption features extracted from an analysis of the galaxy IRAS F0857+3915 and fitting two fifths with similar features extracted directly from Chiar et al. 2006 yielded fits that most closely modelled the data and were closest to being physically plausible.

In our analysis of the distribution of black body temperatures, we found that our system verified that most of the galaxies are best modelled by three black bodies: one cold (<150 K), one warm (>15 K and <500 K) and one hot, (usually >400 K). The variation of temperatures of the cold black bodies was the least, with σ~34 K and rarely reaching above 110 K. The temperature of the warm black bodies were similarly consistent, but having a somewhat greater reach, sometimes dipping below 200 K and sometimes reaching as high as 500 K, but only having σ~150 K. However, the hot black bodies were much more inconsistent, sometimes reaching as low as 300 K and as high as over 1000 K. Yet, this could be due to the fact that we believe some of these incredibly hot black bodies could be heated by an AGN, which could cause the wide range of temperatures.

As for silicate extinction, it appears that the warm black body is most frequently and most strongly affected by silicate absorption, both at the strongest 9.5 μm feature and at the less intense 18 μm feature. This is evident from how there was only an extinction of A_V~0 for about

4% of the warm black bodies and had a very high average of A_V~47. This is drastically different from the cold and hot black bodies, which had silicate extinction of A_V~0 for 35% of cold black bodies and 43% of hot black bodies. Additionally, the average for cold black bodies was A_V~13 and the average for hot black bodies was A_V~21, both of which are significantly lower than the average extinction of the warm black bodies.

The same trend followed with water ice absorption, in that the water ice absorption for warm black bodies was τ~0 only 25% of the sample and the water ice absorption for hot black bodies was zero for as great as ~53% of the sample. Again, the absorption for cold black bodies is negligible, since it only emits minimally from the 4 to 8 μm. This proves to be difficult for QUESTFIT to handle, so we omit it, as it does not affect the fit significantly in any way.

After extracting the PAH emissions, most proved to have at least a minimal presence of PAH emission, with only 3 of the 199 fits lacking any PAH emission.

We also extracted the emission profile of each fitted blackbody and plotted them to be able to further analyze each individually at a later date. In addition, in the future, we hope to analyze correlations between black body temperatures, black body temperatures and silicate absorption, black body temperatures and water ice absorption, each of these with PAH equivalent widths, and etc. Also, we would like to perform a more in depth analysis of the relationships between the various PAH equivalent widths and the total extinction at these wavelengths in order to better determine which galaxies may be AGN dominated and which may be starburst dominated (Veilleux et al. 2009). Similarly, we hope to look more into correlations between water ice absorption and silicate absorption to better determine the structure of the absorbing material and possibly determine the presence of cold molecular clouds (Veilleux et al. 2009).

Works Cited

Chiar, J. E., Tielens A.G.G.M., 2006 ApJ, 637, 774-785

Draine, B. T., Li A., 2001, ApJ, 551, 807-824

Draine, B.T., 2003, ARA&A, 41, 241–289

L´eger, A., Puget, J.L., 1984, A&A 137, L5

Mathis JS, Rumpl W, Nordsieck KH. 1977. Ap. J. 217:425-33

Omont, A. 2007, Reports on Progress in Physics, 70, 1099

Peeters, E., Spoon, H.W.W., Tielens, A.G.G.M., 2004, ApJ 613, 986

Schweitzer, M., et al., 2008, ApJ 679, 101-117

Smith, J.-D., et al., 2007, ApJ 656, 770-791

Spoon, H.W.W., Keane J.V., Tielens A.G.G.M., Lutz D., Moorwood A.F.M., 2001, A&A 365, L353

Spoon, H.W.W., et al., 2004, ApJS 154, 184

Spoon, H.W.W., et al., 2005, Spitzer Observations of Deeply Obscured Galactic Nuclei, IAU symp. 231, 281

Veilleux, S., et al., 2009, ApJS 182, 628-666